# Impact of saline aquifer water on surface and shallow pit corrosion of martensitic stainless steels during exposure to $CO_2$ environment (CCS)



# Impact of saline aquifer water on surface and shallow pit corrosion of martensitic stainless steels during exposure to $CO_2$ environment (CCS)

**Anja Pfennig[1] and Axel Kranzmann[2]**

1 Dept. Mechanical Engineering, Applied Universtiy of Berlin HTW, Berlin, Germany
2 Federal Institute of Materials Research and Testing BAM, Berlin, Germany
E-mail: anja.pfennig@htw-berlin.de

**Abstract.** Pipe steels suitable for carbon capture and storage technology (CCS) require resistance against the corrosive environment of a potential CCS-site, e.g. heat, pressure, salinity of the aquifer, $CO_2$-partial pressure. Samples of different mild and high alloyed stainless injection-pipe steels partially heat treated: 42CrMo4, X20Cr13, X46Cr13, X35CrMo4 as well as X5CrNiCuNb16-4 were kept at T=60 ℃ and ambient pressure as well as p=100 bar for 700 h - 8000 h in a $CO_2$-saturated synthetic aquifer environment similar to possible geological on-shore CCS-sites in the northern German Basin. Main corrosion products are $FeCO_3$ and FeOOH. Corrosion rates obtained at 100 bar are generally much lower than those measured at ambient pressure. Highest surface corrosion rates are 0.8 mm/year for 42CrMo4 and lowest 0.01 mm/year for X5CrNiCuNb16-4 in the vapour phase at ambient pressure. At 100 bar the highest corrosion rates are 0.01 mm/year for 42CrMo4, X20Cr13 (liquid phase), X46Cr13 and less than 0.01 mm/year for X35CrMo4 and X5CrNiCuNb16-4 after 8000 h of exposure with no regard to atmosphere. Martensitic microstructure offers good corrosion resistance.

## 1. Introduction

During the compression of emission gasses e.g. from combustion processes of power plants into deep geological layers of a geological on-shore saline aquifer CCS-site (CCS Carbon Capture and Storage [1]), the corrosion of injection pipe steels may become an issue when $CO_2$ is compressed [2], [3]. $CO_2$-corrosion is sensitively dependent on alloy composition, contamination of alloy and media, temperature, $CO_2$ partial pressure, flow conditions and protective corrosion scales [4]-[10]). Suitable heat treatment [8], [11] and martensitic micro structure [12] decrease the pitting potential. Corrosion phenomena are reason for early failure of materials under cyclic load [13], [14].

Surface corrosion layers grow slowly and locally corroded samples usually show the same corrosion products as surface layers 7], acting as corrosion catalyser. Generally siderite $FeCO_3$ [2] is formed on steels exposed to $CO_2$-environment due to the low solubility of $FeCO_3$ in water (pKsp = 10.54 at 25 ℃ [14]]) leading to anodic iron dissolution. The initial formation of transient $Fe(OH)_2$ [6], [11] possibly leads to an increase of the local pH near the hydroxide film. As a consequence an internal and external ferrous carbonate film precipitates [14]. In this paper we are presenting extended and compiled data of former work [3], [7], [13], [15]-[18].

## 2. Experimental Procedure

*2.1. Steels*

Static corrosion tests at ambient pressure as well as at high pressure (100 bar) were carried out using samples of mild steels, martensitic and duplex stainless steels (Table 1-5):

1. AISI 420 (X20Cr13, 1.4021) (Table 1)
2. AISI 420C (X46Cr13, 1.4043) (Table 2)
3. No AISI (X35CrMo17, 1.4122) (Table 3)
4. AISI 630 (X5CrNiCuNb 16-4, 1.4542) (Table 4)
5. AISI A182 F51 (329LN)) SAF 2205 (X2 CrNiMoN 22-5-3 (UNS S31803) 1.4462) (Table 5)

In order to confirm the material's chemical composition, samples were analyzed via spark emission spectrometry SPEKTROLAB M and by Electron Probe Microanalyzer JXA8900-RLn (Table 1-5).

**Table 1.** Chemical composition of 1.4021 (X20Cr13, AISI 420, (in mass-%).

| Elements | C | Si | Mn | P | S | Cr | Ni | Fe |
|---|---|---|---|---|---|---|---|---|
| | 0.22 | 0.39 | 0.32 | 0.007 | 0.006 | 13.3 | 0.123 | rest |

**Table 2.** Chemical composition of 1.4043 (X46Cr13, AISI 420C), (in mass percent).

| Elements | C | Si | Mn | P | S | Cr | Mo | Ni | Co | Fe |
|---|---|---|---|---|---|---|---|---|---|---|
| | 0.46 | 0.25 | 0.45 | 0.018 | 0.003 | 13.39 | 0.03 | 0.13 | 0.03 | 85.4 |

**Table 3.** Chemical composition of 1.4122 (X35CrMo17), (in mass percent).

| Elements | C | Si | Mn | P | S |
|---|---|---|---|---|---|
| acc standard [a] | 0.33-0.45 | <1.00 | ⩽ 1.00 | ⩽ 0.045 | ⩽ 0.03 |

| Elements | Cr | Mo | Ni | Co | Fe |
|---|---|---|---|---|---|
| acc standard [a] | 15.5 – 17.5 | 0.8-1.3 | ⩽ 1.00 | | 0.20 – 0.45 |

a) elements as specified according to DIN EN 10088-3 in %

**Table 4.** Chemical composition of 1.4542 (X5CrNiCuNb16-4, AISI 630), (in mass percent).

| Elements | C | Si | Mn | P | S | Cr | Mo | Ni | Cu | Nb |
|---|---|---|---|---|---|---|---|---|---|---|
| | 0.03 | 0.42 | 0.68 | 0.018 | 0.002 | 15.75 | 0.11 | 4.54 | 3.00 | 0.242 |

Duplex steel 1.4462 (X2 CrNiMoN 22 5 3, (table 5) manufactured by means of continuous casting followed by an appropriate tempering and water quenching allowing for an equilibrium of ferrite and austenite phase. Due to its percentage of austenite 1.4462 reveals a much better corrosion resistance resulting and a PREN number (35.1) twice as high as 1.4542 [16].

**Table 5.** Chemical composition of 1.4462 X2 CrNiMoN 22 5 3 (UNS S31803) (in mass percent).

| phases | C | Si | Mn | Cr | Mo | Ni | N |
|---|---|---|---|---|---|---|---|
| α & γ ** | 0.023 | 0.48 | 1.83 | 22.53 | 2.92 | 5.64 | 0.15 |

*PREN α =37,4, γ =32,4 ** P=0.024, S=0.008

*2.2. Aquifer Water*

To simulate in-situ geothermal condition the geothermal aquifer water (as known to be similar to the Stuttgart Aquifer [19], [20]: $Ca^{2+}$: 1760 mg/L, $K^{2+}$: 430 mg/L, $Mg^{2+}$: 1270 mg/L, $Na^{2+}$: 90100 mg/L, $Cl^{-}$: 143,300 mg/L, $SO_4^{2-}$: 3600 mg/L, $HCO_3^{-}$: 40 mg/L) was synthesized in a strictly orderly way to avoid precipitation of salts and carbonates.

*2.3. Corrosion Experiments*

Laboratory scale exposure tests in $CO_2$-saturated aquifer brine and water saturated $CO_2$ were carried out using coupons of the steel qualities that may be used as injection pipe. Therefore steel samples made of as received and thermally treated specimens with 8 mm thickness, 20 mm width, 50 mm length were used. To gain martensitic microstructure with sufficient hardness and toughness prior to exposure heat treatment was done following commonly used protocols [7], [15], [17].

A hole of 3.9 mm diameter was used for sample positioning. Samples of each base metal were positioned within the vapour phase and within the liquid phase. Flow control (3 NL/h) of the technical $CO_2$ (purity 99.995 vol.-%)) into the brine at ambient pressure was done by a capillary meter GDX600_man by QCAL Messtechnik GmbH, Munich. The exposure of the samples between 700 h to 8000 h was disposed in reaction vessels according to the conditions at the geological site at 60 ℃ at ambient pressure – each material in a separated reaction vessel [3] and at 100 bar [7], [13], [15] (Figure 1).

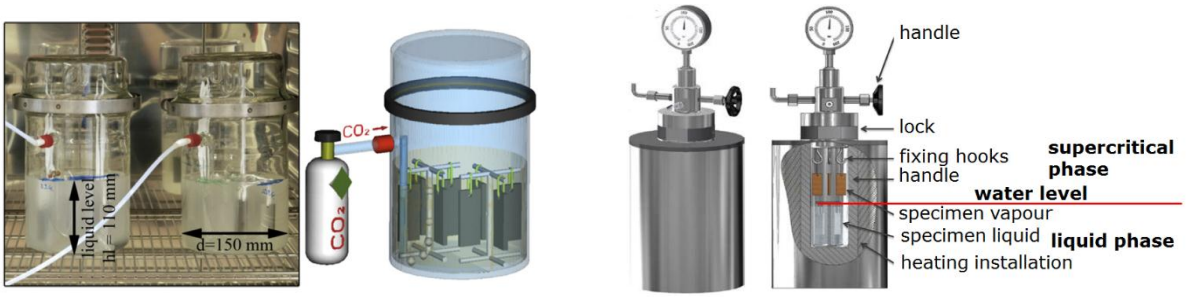


**Figure 1.** Reaction vessels and experimental set up [7], [17].

Before corrosion tests the surfaces of the steels were activated by grinding with SiC-Paper down to 120 µm under water. After the corrosion tests, the samples were cut partly for scale analysis with the corrosion layer and prepared partly for kinetic analysis after the scale was etched. Descaling of the samples was performed by exposure to 37% HCl. Then parts of the samples were embedded in a cold resin (Epoxicure, Buehler), cut and polished first with SiC-Paper from 180 µm to 1200 µm under water and then finished with diamond paste 6 µm and 1 µm.

*2.4. Analysis*

Different light optical and electron microscopy techniques were performed on specimens to investigate the layer structures and morphology of the samples. X-ray diffraction was carried out in a URD-6 (Seifert-FPM) with $CoK_\alpha$-radiation with an automatic slit adjustment, step 0.03 ° and count 5 sec. Phase analysis was performed by matching peak positions automatically with PDF-2 (2005) powder patterns. Mainly structures that were likely to precipitate from the steels were chosen of the ICSD and refined to fit the raw-data-files using POWDERCELL 2.4 [21] and AUTOQUAN ® by Seifert FPM. Kinetics of the corrosion were determined by the corrosion rates which were calculated via mass change of the samples before and after corrosion testing according to DIN 50 905 part 1-4.

$$corrosion\ rate\left[\frac{mm}{year}\right]=\frac{8760\left[\frac{hours}{year}\right]\cdot 10\left[\frac{mm}{cm}\right]\cdot weight\ loss[g]}{area\left[cm^2\right]\cdot density\left[\frac{g}{cm^3}\right]\cdot time[hour]} \quad (1)$$

## 3. Results and Discussion

As expected due to the high PREN (53.1 (Pitting Resistance Equivalent (PRE = %Cr + 3.3% Mo + 16% N)) for the duplex stainless steel X2 CrNiMoN22-5-3 is reason for no corrosion phenomena at all, even after long exposure times in Stuttgart Aquifer water [19] and Northern German Basin [20] with

or without flowing technical $CO_2$. Neither ferrite nor austenite phase showed corrosive deterioration (Figure 2). Molybdenum specially increases the resistance to pitting and crevice corrosion.

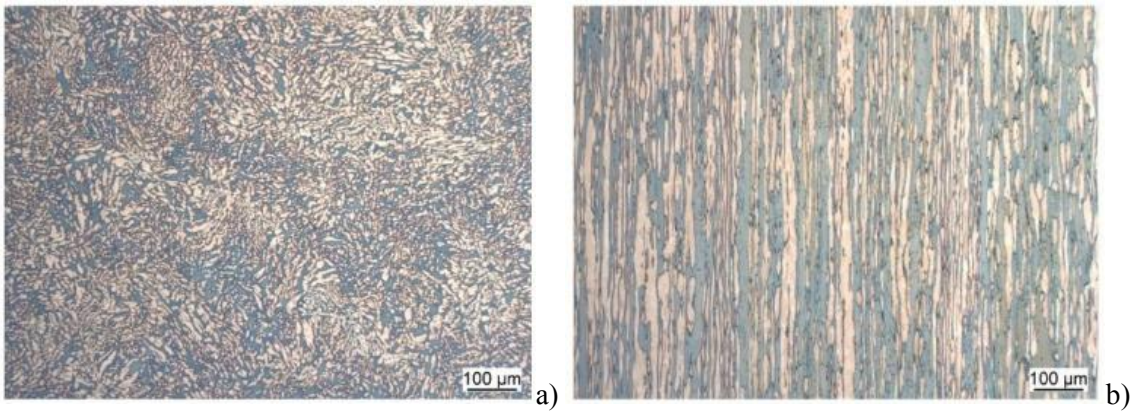


a) b)

**Figure 2.** Microstructure of experimental alloy prior to testing; (a) transversal and (b) longitudinal sections respecting the casting direction. Etching: Beraha II [19].

In general corrosion rates are lower at 100 bar compared to ambient pressure. This applies for mild steel 42CrMo4 (Figure 3) as well as for martensitic stainless steels X46Cr13 (Figure 4), X35CrMo17 (Figure 5) and X5CrNiCuNb 16-4 (Figure 6). Corrosion rates are higher at ambient pressure than at 100 bar, which may directly be related to an open capillary system within the corrosion layer. Under pressure these are not present suppressing fast mutual diffusion of ionic species that is necessary for scale growth [18]. The corrosion rates of 42CrMo4, X20Cr13 and X46Cr13 increase with time at ambient pressure and decrease with time at 100 bar. X5CrNiCuNb16-4 and X35CrMo17 show increasing corrosion rates at ambient pressure as well as at 100 bar [18].

One reason for the decreasing corrosion rates lower gas tightness of the low pressure system with excess oxygen in the test vessels at ambient pressure leading to higher corrosion rates as a function of exposure time. Decreasing growth rates at 100 bar may be related to the fast formation of initial hydroxides [2], [6], [14], [18] then precipitating to a passivating siderite-layer with increasing thickness as a function of exposure time. This corrosion scale acts as a diffusion barrier towards mutual diffusion of ionic species to the metal surface. The corrosion rate may also decrease in the presence of iron carbonate precipitates and explains lower corrosion rates at longer exposure times.

In general corrosion rates are severely dependent on the exposure time t for specimens kept in the vapour phase. For example the corrosion rate is twice as high for 42CrMo4 after 8000 h (0.8 mm/year) in comparison to 4000 h (0.45 mm/year) when exposed at ambient pressure. This effect has less impact on specimens kept in the liquid phase or at 100 bar with no regard to atmosphere [18]. However, the atmosphere (liquid, vapour or supercritical atmosphere) does not significantly influence the general corrosive behavior.

The pressure has little influence on the corrosion rates. For 42CrMo4, X20Cr13 and X35CrMo4 the corrosion rates at ambient pressure are much higher than at 100 bar. For X20Cr13 and X5CrNiCuNb16-4 the difference is not as significant. In general the higher corrosion rates at ambient pressure may be explained by higher diffusion kinetics. The corrosion rates in the vapour phase (water-saturated $CO_2$) exceed those measured in the liquid phase ($CO_2$-saturated water) by a factor of 3–8. But, at high pressures (100 bar) corrosion rates in the liquid phases can be higher or lower than in the vapour/supercritical phase.

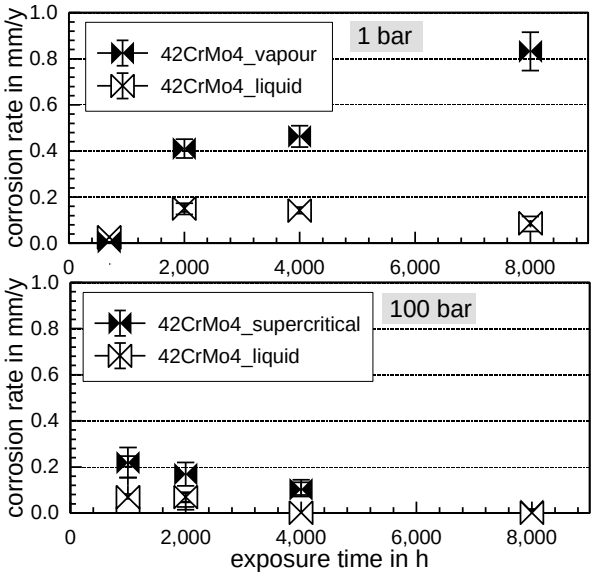


**Figure 3.** Comparison of corrosion rates of 42CrMo4 after 8000 h of exposure to aquifer brine water at 60 ℃ and ambient pressure [3] as well as at 100 bar [18].

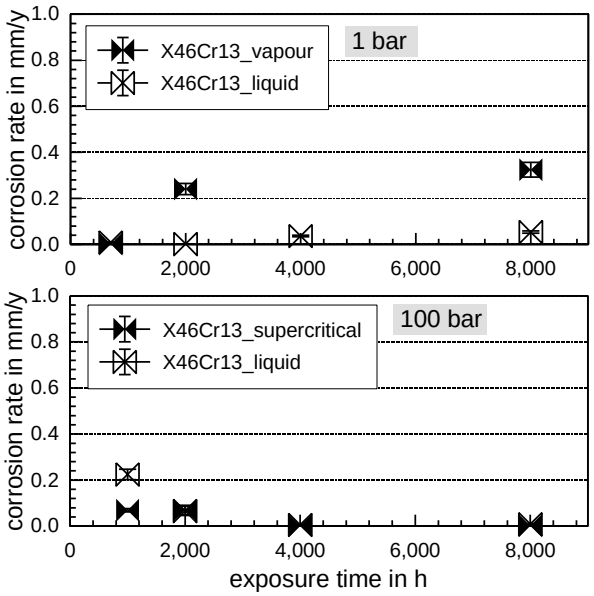


**Figure 4.** Comparison of corrosion rates of X20Cr13 in the liquid and vapour/supercritical phase after 8000 h of exposure to aquifer brine water at 60 ℃ and ambient pressure as well as at 100 bar.

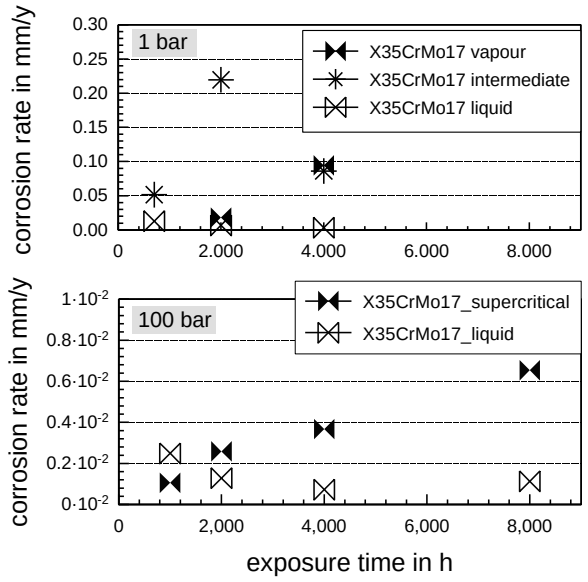


**Figure 5.** Comparison of corrosion rates of X46Cr13 in the liquid and vapour/supercritical phase after 8000 h of exposure to aquifer brine water at 60 ℃ and ambient pressure [3] as well as at 100 bar [18].

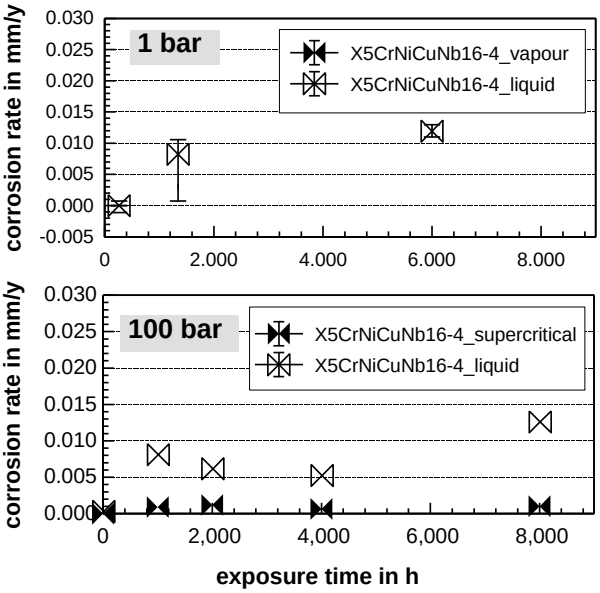


**Figure 6.** Comparison of corrosion rates of X35CrMo17 in the liquid and vapour/supercritical phase after 8000 h of exposure to aquifer brine water at 60 ℃ and ambient pressure as well as at 100 bar.

However, the corrosion rates for 42CrMo4 are higher in the liquid/vapour phase and also higher at ambient pressure compared to high pressure. This corresponds with the thickness of the precipitation layer that is greater in vapour/supercritical than in the liquid phase (Figure 3 and Figure 7).

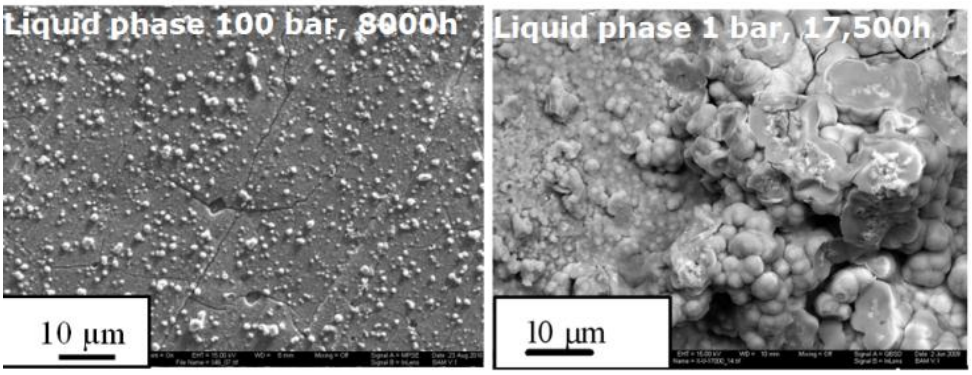


**Figure 7.** Surface precipitation on 42CrMo4 after exposure to $CO_2$ saturated saline aquifer water for 8000 h at ambient pressure and 100 bar.

The multi-layered corrosion scale precipitated on the steels at ambient pressure is complicated and has been described in detail [7], [17], [18]. This characteristic carbonate/oxide structure consists of siderite $FeCO_3$, goethite a-FeOOH, mackinawite FeS and akaganeite $Fe_8O_8(OH)_8Cl_{1.34}$ and in addition spinel-phases of various compositions. Carbides, such as $Fe_3C$ or chromium-rich iron carbides were visible within the corrosion layer.

## 4. Conclusion

Immersion tests at 60°C at ambient pressure and at 100 bar were performed in saline aquifer water (Stuttgart Aquifer and Northern German Basin) at 60 °C using technical $CO_2$ to model the CCS-environment. According to DIN 6601 42CrMo4, X20Cr13 and X46Cr13 would be unsuitable for pressure vessel application, when being surrounded by the $CO_2$-saturated brine at ambient pressure.
The following conclusions for the corrosion for corrosion phenomena of different steels may be stated:

i. Main corrosion products of a continuous corrosion scale as well as pits after static corrosion tests at ambient pressure as well as 100 bar were $FeCO_3$ and FeOOH for all steel qualities. Corrosion reactions are diffusion controlled with slower diffusion in the liquid phase leading to increased siderite crystal sizes than in the vapour/supercritical phase (smaller crystals due to higher diffusion rates).
ii. Corrosion rates obtained at 100 bar are generally much lower after 8000 h of exposure than those measured at ambient pressure (depending on the atmosphere (vapour or liquid) by a factor of ca. 10–80 for 42CrMo4, a factor of ca. 1.5–30 for X46Cr13, a factor of ca. 10–100 for X20Cr13 and a factor of ca. 10 for X35CrMo17-1, exception for X5CrNiCuNb16-4 with similar surface corrosion rates in the liquid phase).
iii. Highest surface corrosion rates are 0.8 mm/year for 42CrMo4 (1% Cr), 0.3 mm/year for X46Cr13 (13% Cr), 0.3 mm/year for X20Cr13 (13% Cr), 0.1 mm/year for X35CrMo17-1 (17% Cr) and 0.01 mm/year for X5CrNiCuNb16-4 (16% Cr) in the vapour phase at ambient pressure after 8000 h of exposure. At 100 bar the highest corrosion rates are 0.01 mm/year for 42CrMo4, X20Cr13 (liquid phase) X46Cr13 and less than 0.01 mm/year for X35CrMo4 and X5CrNiCuNb16-4 after 8000 h of exposure with no regard to atmosphere.
iv. The carbon content does not show significant influence on corrosion rate. But higher chromium content results in lower surface corrosion rates and therefore better corrosion resistance. Due to high Cr, Ni and Mo content X2CrNiMoN 22-5-3 shows now surface corrosion at all under the conditions given.

## 5. References

[1] Van den Broek, Hoefnagels M R, Rubin E, Turkenburg, W and Faaij, E, Effects of technological learning on future cost and performance of power plants with $CO_2$ capture, in Projects Costs of Generating Electricity 2010 Progress in Energy and Combustion Science 177-187, ISBN 978-92-64-08430-8

[2] Nešić S 2007 Key issues related to modelling of internal corrosion of oil and gas pipelines – A review *Corrosion Science* 49 4308–4338

[3] Pfennig A and Kranzmann A 2011 Reliability of pipe steels with different amounts of C and Cr during onshore carbon dioxide injection *International Journal of Greenhouse Gas Control* 5 757–769

[4] Zhang H, Zhao Y L and Jiang Z D 2005 Effects of temperature on the corrosion behaviour of 13Cr martensitic stainless steel during exposure to CO2 and Cl- environment *Material Letters* 59 3370-3374

[5] Alhajji J N and Reda M R 1993 The effect of alloying elements on the electrochemical corrosion of low residual carbon steels instagnant $CO_2$-saturated brine *Corrosion Science* 34 1899-1911

[6] Choi Y S and Nešić S 2008 Corrosion behaviour of carbon steel in supercritical $CO_2$-water environments, No. 09256 *NACE Corrosion Conference and Expo*, New Orleans, Louisiana, USA, March 16th – 20th

[7] Pfennig A, Zastrow P and Kranzmann A 2013 Influence of heat treatment on the corrosion behaviour of stainless steels during $CO_2$-sequestration into saline aquifer *International Journal of Green House Gas Control* 15 213–224

[8] Bülbül Ş and Sun Y 2010 Corrosion behaviours of high Cr-Ni cast steels in the HCl solution, *Journal of Alloys and Compounds* 598 143-147

[9] Banaś J, Lelek-Borkowska U, Mazurkiewicz B and Solarski W 2007 Effect of $CO_2$ and $H_2S$ on the composition and stability of passive film on iron alloy in geothermal water *Electrochimica Acta* 52 5704–5714

[10] Wei L, Pang X, Liu C and Gao K 2015 Formation mechanism and protective property of corrosion product scale on X70 steel under supercritical $CO_2$ environment *Corrosion Science* 100 404–420.

[11] Isfahany A N, Saghafian H and Borhani G 2011 The effect of heat treatment on mechanical properties and corrosion behaviour of AISI420 martensitic stainless steel *Journal of Alloys and Compounds* 509 3931-3936

[12] Lucio-Garciaa M A, Gonzalez-Rodrigueza J G, Casalesc M, Martinezc L, Chacon-Navaa J G, Neri-Floresa M A and Martinez-Villafañea A 2009 Effect of heat treatment on $H_2S$ corrosion of a micro-alloyed C–Mn steel *Corrosion Science* 51 2380-2386

[13] Pfennig A, Wiegand R, Wolf M and Bork C-P 2013 Corrosion and corrosion fatigue of AISI 420C (X46Cr13) at 60 °C in CO2-saturated artificial geothermal brine *Corrosion Science* 68 134–143

[14] Han J, Yang Y, Nešić S and Brown B N 2008 Roles of passivation and galvanic effects in localized $CO_2$ corrosion of mild steel, Paper No. 08332, NACE Corrosion 2008, New Orleans, Louisiana, USA, March 16th – 20th

[15] Pfennig A, Wolthusen H and Kranzmann A 2017 Unusual corrosion behavior of 1.4542 exposed a laboratory saline aquifer water CCS-environment *Energy Procedia* 114 5229-5240

[16] Wolf M, Afanasiev R, Böllinghaus Th and Pfennig A 2017 Investigation of Corrosion Fatigue of Duplex Steel X2CrNiMoN22 5 3 Exposed to a Geothermal Environment under Different Electrochemical Conditions and Load Types *Energy Procedia* 114 5337-5345

[17] Pfennig A, Wolthusen H, Wolf M and Kranzmann A 2014 Effect of heat treatment of injection pipe steels on the reliability of a saline aquifer water CCS-site in the Northern German Basin *Energy Procedia* 63 5762-5772

[18] Pfennig A and Kranzmann A 2012 Effect of $CO_2$ and pressure on the stability of steels with different amounts of Chromium in saline water *Corrosion Science* 65 441–452

[19] Förster A, Norden B, Zinck-Jørgensen K, Frykman P, Kulenkampff,J, Spangenberg, E, Erzinger J, Zimmer M, Kopp J, Borm G, Juhlin C, Cosma C and Hurter S 2006 Baseline characterization of the $CO_2$SINK geological storage site at Ketzin, Germany *Environmental Geosciences* 13 145-161
[20] Förster A et al. 2010 Reservoir characterization of a $CO_2$ storage aquifer: The Upper Triassic Stuttgart Formation in the Northeast German Basin *Mar. Pet. Geol.* 27 2156–2172
[21] Kraus S W and Nolze G 1996 POWDER CELL – a program for the representation and manipulation of crystal structures and calculation of the resulting X-ray powder patterns *J. Appl. Cryst.* 29 301-303

**Acknowledgment**
This work was supported by the FNK (Fachkonferenz für wissenschaftliche Nachwuchskräfte) of the Applied University of Berlin, HTW and by IMPACT (EU-Project EFRE 20072013 2/21).